# Fractional Fourier Transform Receiver for Modulated Chirp Waveforms

Petrov, N.; Yarovoy, Alexander

**DOI**
10.1109/TMTT.2022.3222225

**Publication date**
2022

**Document Version**
Accepted author manuscript

**Published in**
IEEE Transactions on Microwave Theory and Techniques

# Fractional Fourier Transform Receiver for Modulated Chirp Waveforms

Nikita Petrov* and Alexander Yarovoy†
Microwave Sensing, Signals and Systems (MS3)
Delft University of Technology
Mekelweg 4, 2628 CD, Delft, the Netherlands
E-mails: *N.Petrov@tudelft.nl, †A.Yarovoy@tudelft.nl

***Abstract*—A novel receiver structure for the reception of linearly frequency modulated (LFM) chirps carrying additional narrow-band (phase) modulation is proposed. A linear relation between the time delay and the beat frequency shift of the target response in stretch processing is exploited to estimate the target range via correlation of the received signal with the replica in a Fractional Fourier Transform (FrFT) domain. According to numerical simulations, the proposed FRFT receiver demonstrates improved performance and computational efficiency over the state-of-the-art solutions for the moderate-to-large bandwidth of the information-carrying modulation. The receiver was integrated into the waveform-agile radar PARSAX and its performance has also been verified experimentally.**

***Index Terms*—Linear frequency modulation (LFM), phase-coded FMCW, automotive radar, fractional Fourier transform (FrFT), fractional correlation, radar signal processing.**

## I. Introduction

A linearly frequency modulated (LFM) waveform has been widely used in various radar applications for decades. The simplicity of the hardware with low requirements on analogue to digital converter (ADC) sampling frequency, constant peak-to-average power ratio (PAPR) and good Doppler tolerance are the key advantages of the LFM waveform. These advantages come with the cost of the limited flexibility of LFM signals, crucial for the realization of multiple-input multiple-output (MIMO) radars and interference mitigation between different radars. To associate the received signals with the proper transmit channel, different multiplexing schemes are used in MIMO radars. They imply that the transmitted signals are different in time, frequency, chirp slope or code domains, but at the same time lead to the degradation of radar performance by shortening the unambiguous Doppler velocity, degrading the range resolution or increasing the sidelobe level [1].

A promising approach to address the aforementioned limitations consists of applying information-carrying modulation to chirps. In that way, the received waveform can be processed after mixing with the reference LFM signal (known as dechirping, deramping and stretch processing) – preserving all the advantages of LFM signal mentioned above, and adding to them the ability to discriminate different signals, essential for MIMO beam-forming, interference mitigation between different radars, and realization of joint communication and sensing.

The initial research on applying phase modulation to chirps was carried in [2], [3] and some insight in the sensing capabilities of such modulation was given in [4]. A filter-bank receiver structure to deal with phase-modulated FMCW waveform was proposed in [5], [6]. Therein the authors noticed that the received signal after dechirping has a time delay and the beat frequency shift proportional to the range to the target. To consider these two effects together, the authors proposed the compensated stretch processing [5], [6], which takes both these effects into account. The implementation of the compensated stretch processing requires applying a filter bank for all ranges of interest. Therefore it has the computational complexity of digital Fourier transform (DFT) $\mathcal{O}(N^2)$, where $N$ is the number of samples per chirp at $f_s$. That is significantly larger than that of the standard dechirping realized via the fast Fourier transform (FFT): $\mathcal{O}(N \log_2(N))$. Thus, high computational complexity of the compensated stretch processing makes challenging its realization on low cost FMCW radar applications, e.g. an automotive radar chip.

The state-of-the-art approaches to process phase-modulated FMCW waveforms [7]–[10] use the group delay filter in the receiver to align the responses at all range cells before decoding, followed by FFT for range extraction. The original idea of such delay compensation comes from the correction of non-linearity of chirp slope for stretch processing, e.g. [11]–[13]. This receiver design, derived with an assumption of a narrow-band deviation of the signal from the linear frequency modulation (LFM), significantly degrades for long codes (modulation signals with the bandwidth comparable to the beat signal ADC sampling frequency), which are of the main interest in applications mentioned above. An appropriate predistortion of the transmit signal to compensate for this effect has been proposed [14], [15], which, however, leads to an increase in the PAPR of the transmitted signal, undesirable for the transmission chain.

A conceptually similar approach is proposed in [16] with application to chirps modulated by an orthogonal frequency division multiplexing (OFDM) waveform. Instead of the group delay filter, they propose a certain rearrangement of the OFDM sub-carriers to realize a symbol canceling receiver. This, however, imposes multiple constraints on the selection of the waveform parameters.

In this paper, we propose a novel receiver design for modulated LFM signals, which demonstrates the ability to recover the range profile accurately, similar to the compensated stretch processing, and does so in the computational complexity of

FFT. To do that, we present in Section II-A the signal model and derive the matched filter receiver, which coincides with the compensated stretch processing [5], [6]. It is further shown that due to the linear relation between the time delay and the beat frequency, the matched filter can be realized via the fractional correlation [17], [18], which can be computed efficiently using the fractional Fourier transform (FrFT) with the computational load of FFT [18], [19]. Consequently, in Section III we propose a received based on fractional correlation. The performance of the proposed receiver is compared to the other state-of-the-art solutions through numerical simulations in Section IV and via processing of measured radar data in Section V. Finally, the conclusions are drawn in Section VI.

## II. Signal model and matched filter receiver

### A. Signal model

Assume that the radar transmits a wideband LFM chirp modulated with a narrow-band modulation signal $m(t)$:

$$s_{\mathrm{t}}(t) = m(t)e^{-j2\pi\left(f_{\mathrm{c}}t+\frac{\beta t^2}{2}\right)}, \quad t \in [0, T], \tag{1}$$

where $f_{\mathrm{c}}$ stands for the carrier frequency of the radar, $\beta = B/T$ is the chirp rate, $B$ and $T$ are the bandwidth of the duration of the chirp respectively. Moreover, we assume that the bandwidth of $m(t)$ is much smaller than that of the chirp $B_{\mathrm{m}} \ll B$.

The signal (1) impinges on a target at a range $r_0$ moving with a constant radial velocity $v_0$ towards or away from the radar. The reflected signal is received by the radar with a time delay:

$$\tau_0(t) = \frac{2}{c}\left(r_0 + v_0 t\right) = \tau_0 + \frac{2v_0}{c}t \tag{2}$$

attenuated proportionally to the target RCS and two-way propagation of the way by the complex coefficient $\alpha_0$. Hereafter, we incorporate all constant terms of signal processing into $\alpha_0$ with no loss of generality. The signal impinging the receiver becomes:

$$\begin{aligned} s_{\mathrm{r}}(t) &= \alpha_0 s_{\mathrm{t}}(t-\tau_0(t)) = \\ &\alpha_0 m\left(\left(1-\frac{2v_0}{c}\right)t-\tau_0\right)e^{-j2\pi f_{\mathrm{c}}\left(1-\frac{2v_0}{c}\right)t} \\ &\cdot e^{j2\pi f_{\mathrm{c}}\tau_0}e^{-j2\pi\frac{\beta}{2}\left(t\left(1-\frac{2v_0}{c}\right)-\tau_0\right)^2} \\ &\approx \alpha_0 m\left(t-\tau_0\right)\cdot e^{-j2\pi\left(f_{\mathrm{c}}t-f_{\mathrm{D}}t+\frac{\beta}{2}\left(t^2-2t\tau_0\right)\right)}, \end{aligned} \tag{3}$$

where $f_{\mathrm{D}} = 2v_0 f_{\mathrm{c}}/c$, the constant phase terms are substituted into $\alpha_0$ and we used $(1 - 2v_0/c) \approx 1$ considering that the velocities typical of automotive scenarios satisfy $v_0 \ll c$. Applying the stretch processing on receive, which consists of multiplication of the received signal with the transmitted chirp and filtering out high-frequency components, results in:

$$\begin{aligned} s(t) &= s_{\mathrm{r}}(t)e^{j2\pi\left(f_{\mathrm{c}}t+\frac{\beta t^2}{2}\right)} \\ &= \alpha_0 m\left(t-\tau_0\right)e^{j2\pi(\beta\tau_0+f_{\mathrm{D}})t} \\ &\approx \alpha_0 m\left(t-\tau_0\right)e^{j2\pi\beta\tau_0 t}. \end{aligned} \tag{4}$$

It comprises two main components: the delayed modulated signal and the beat frequency. The second item is standard for dechirping of LFM signals. It also comprises Doppler frequency shift due to target motion, which is typically negligible compared to the frequency resolution of the beat signal after applying FFT to it, i.e. $f_{\mathrm{D}} \ll f_{\mathrm{s}}/N$, where $f_{\mathrm{s}}$ is the sampling frequency of the beat signal and $N$ is the number of fast-time samples.

### B. Signal processing - filter bank

The form of (4) can be alternatively interpreted if we denote $f_{\mathrm{VD}} = \beta\tau_0$ as a virtual Doppler frequency shift, which is significantly (about two orders of magnitude) larger than the typical Doppler frequency shift for automotive radars $f_{\mathrm{D}}$ in (4). In this formulation, it resembles a conventional response of a waveform $m(t)$ with the time delay $\tau_0$ and the Doppler frequency shift $f_{\mathrm{VD}}$. This representation is similar to the reception of a general waveform $m(t)$ with a large Doppler shift. In this case, the optimal receiver in white noise is a matched filter for each range-Doppler hypothesis [20]. It can be realized either via a search over all possible range-Doppler bins or via performing Doppler processing prior to range compression. Due to the explicit relation between the parameters $f_{\mathrm{VD}} = \beta\tau_0$, a one-dimensional search is needed on the parameter $\tau$. Thus, the receiver calculates for each $\tau$:

$$y(\tau) = \int s(t)m^*\left(t-\tau\right)e^{-j2\pi\beta\tau t}dt. \tag{5}$$

Modern radars perform baseband signal processing digitally, after the received beat signal is sampled by ADC at the sampling frequency $f_{\mathrm{s}}$ and stored in vector $\mathbf{s} \in \mathbb{C}^{N\times 1}$:

$$\mathbf{s} = \alpha_0 m\left(n/f_{\mathrm{s}}-\tau_0\right)e^{j2\pi\beta\tau_0 n/f_{\mathrm{s}}}, \tag{6}$$

where $t = n/f_{\mathrm{s}}, n = 0, \ldots, N-1$.

The reference signal in the integral (5) for the fixed $\tau$ can be given via a Hadamard product of two vectors $\mathbf{a}(\tau)\odot\mathbf{m}(\tau)$:

$$\begin{aligned} \mathbf{a}(\tau) &= e^{j2\pi\beta\tau n/f_{\mathrm{s}}}, \\ \mathbf{m}(\tau) &= m\left(n/f_{\mathrm{s}}-\tau\right), \end{aligned} \tag{7}$$

$n = 0, \ldots, N-1$; $\mathbf{a}(\tau), \mathbf{m}(\tau) \in \mathbb{C}^{N\times 1}$.

Stacking the steering vectors of the beat signal and the delayed modulation signal as columns in matrices $\mathbf{A} = [\mathbf{a}(\tau_0), \ldots, \mathbf{a}(\tau_{N_r})]$ and $\mathbf{M} = [\mathbf{m}(\tau_0), \ldots, \mathbf{m}(\tau_{N_r})]$ respectively, with $N_r$ being the predefined number of range cells, it is possible to write the convolution (5) via a vector product:

$$\mathbf{y} = \left(\mathbf{A}\odot\mathbf{M}\right)^H\mathbf{s}. \tag{8}$$

This receiver structure has previously been proposed in [5], [6] and is called compensated stretch processing. The compensation referred to in the name of the algorithm realizes the proper shift of the reference modulation signal for each range hypothesis, realized here via matrix $\mathbf{M}$. Filter bank realization of compensated stretch processing leads to the computational complexity of DFT $\mathcal{O}(N^2)$.

### C. Waveform analysis and design

The key block of the receiver (5) (or its digital counterpart (8)) correlates the received signal with the time delay and frequency shifted template. This is equivalent to calculating the cross-correlation of $s(t)$ and $m(t)$ along the diagonal line in the time delay / Doppler shift domain. If we further expand (5), considering the target Doppler frequency shift as in (4), we get:

$$\begin{aligned} y(\tau) &= \alpha_0 \int m\left(t-\tau_0\right) m^*\left(t-\tau\right) e^{-j2\pi(\beta(\tau-\tau_0)-f_{\mathrm{D}})t} dt \\ &= \alpha_0 \int m\left(t'\right) m^*\left(t'-\Delta_\tau\right) e^{-j2\pi(\beta\Delta_\tau-f_{\mathrm{D}})t'} dt' \\ &= \alpha_0 \chi_m\left(\Delta_\tau, -\left(\beta\Delta_\tau - f_{\mathrm{D}}\right)\right), \end{aligned} \tag{9}$$

where $t' = t - \tau_0$, $\Delta_\tau = \tau - \tau_0$ and $\chi_m(\tau, f_D)$ defines the ambiguity function of the waveform $m(t)$; the constant phase term $e^{-j2\pi(\beta\Delta_\tau - f_{\mathrm{D}})\tau_0}$ was substituted into $\alpha$ with no loss of generality. It implies that the range response of the proposed processing is determined by the diagonal cut of the ambiguity function $\chi_m(\tau, f_{\mathrm{D}})$. This can be alternatively interpreted as a shear of the ambiguity function of the waveform $m(t)$ being modulated by a chirp [21]. Another consequence of (9) is that the (phase) modulation schemes, optimized for low range sidelobes, e.g Barker, Frank or Zadoff-Chu phase codes [21], would not preserve this property if they are used to modulate a chirp (1). The design of optimal modulation schemes to be applied for the proposed receiver structure is the subject of ongoing research.

## III. Fractional correlation receiver

In a conventional radar signal processing, the time delay (range) and signal frequency shift (Doppler) are typically estimated separately and independent of each other: range via the correlation of the received signal with the replica and Doppler frequency via Fourier transform over slow-time – both with a computational complexity of FFT. The former exploits the fact that correlation in time transforms into a simple multiplication operation in the frequency domain [22]:

$$\begin{aligned} s(t) \circledast m^*\left(t-\tau\right) &= \int s(t) m^*\left(t-\tau\right) dt \\ &= \mathcal{F}^{-\frac{\pi}{2}}\left\{S(f) M^*(f)\right\}, \end{aligned} \tag{10}$$

where $\circledast$ denotes correlation, $\mathcal{F}^{-\frac{\pi}{2}}\{\cdot\}$ is the inverse Fourier transform (the reason for this superscript will be explained shortly); $S(f)$ and $M(f)$ are the Fourier transforms of $s(t)$ and $m(t)$ respectively.

Therefore, the objective is to develop an efficient algorithm to calculate the cross-correlation along the diagonal line in the time delay / Doppler frequency shift domain (5) with the computational complexity of FFT. This can be done using the theory of fractional Fourier transform (FrFT) and fractional correlation [23], [24]. Recently FrFT has been widely used in numerous signal processing applications [17], [25], including radar, where it has been applied to focus (inverse) synthetic aperture radar ((I)SAR) images [18], passive radar signal processing [25], coherent integration of moving target over long time intervals [26] and waveform design [27].

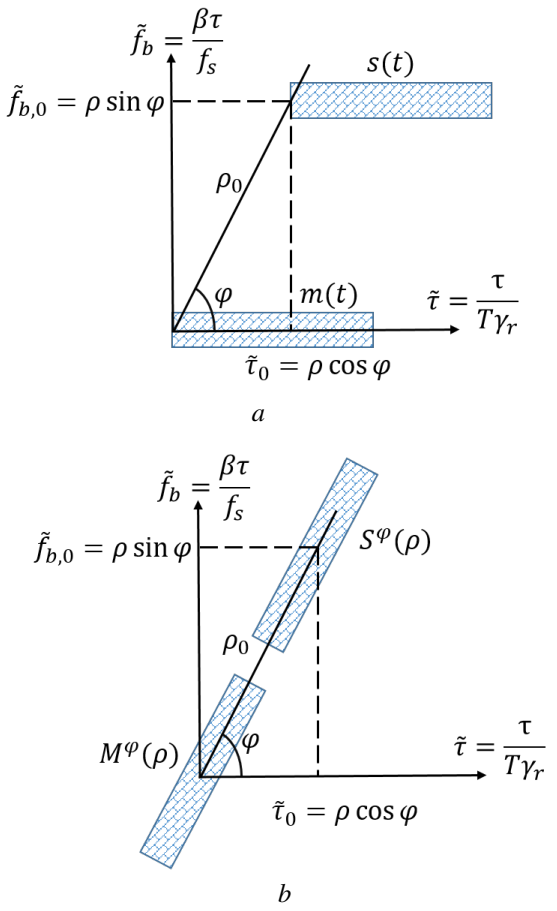


Fig. 1. Time-frequency representation of the received signal and its relation to the FrFT angle $\varphi$: (*a*) before FrFT, (*b*) after FrFT.

With the use of FrFT, the definition (10) can be extended to calculate the cross-correlation along any line in the Doppler-delay plane [24]:

$$\begin{aligned} y(\tau) &= s(t) \circledast^{\varphi} m^*\left(t-\tau\right) \\ &= \mathcal{F}^{-\frac{\pi}{2}}\left\{S^{\frac{\pi}{2}+\varphi}(\rho)\left(M^{\frac{\pi}{2}+\varphi}(\rho)\right)^*\right\}, \end{aligned} \tag{11}$$

where the operators $\circledast^{\varphi}$ and $\mathcal{F}^{\varphi}\{\cdot\}$ denotes fractional correlation and the fractional Fourier transform associated with angle $\varphi$, measured anti-clockwise from the time axis, such that $\mathcal{F}^{\frac{\pi}{2}}\{\cdot\}$ and $\mathcal{F}^{-\frac{\pi}{2}}\{\cdot\}$ correspond to the Fourier transform and inverse Fourier transform respectively. Moreover, we denote by $S^{\varphi}(\rho) = \mathcal{F}^{\varphi}\{s(t)\}$ and $M^{\varphi}(\rho) = \mathcal{F}^{\varphi}\{m(t)\}$ the $\varphi$-th fractional Fourier transform (FrFT) of $s(t)$ and $m(t)$ [17], [18], [23] and $\rho$ is the argument in this FrFT domain.

The fractional Fourier transform (FrFT) of $s(t)$ is defined for angle $\varphi$ as [24, eq. (9)]:

$$\begin{aligned} S^{\varphi}(\rho) &= \sqrt{1 - j\cot\varphi} e^{j\pi\rho^2\cot\varphi} \\ &\cdot \int s(t) e^{j\pi t^2\cot\varphi - j2\pi t\rho\csc\varphi} dt. \end{aligned} \tag{12}$$

The time-frequency representation of the modulation signal $m(t)$ and that of the received signal (4) are presented in Fig. 1 before (*a*) and after (*b*) applying FrFT to them. It can be seen that the target range information is fully described by the radial displacement $\rho$ at the angle $\varphi$. It was shown in [24,

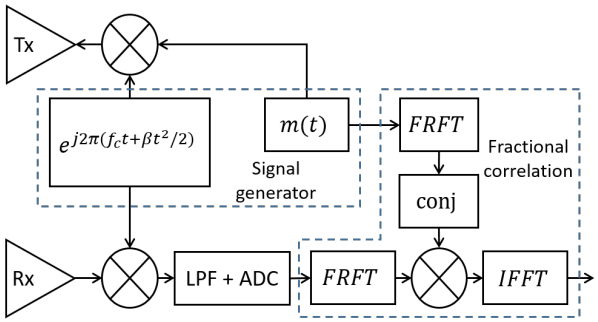


Fig. 2. FRFT receiver structure for modulated FMCW waveforms

eq. (21)] that the displacement of the signal time-frequency representation by $\rho, \varphi$ in polar coordinated corresponds to:

$$S^{\varphi}(\rho - \rho_0) = \mathcal{F}^{\varphi}\{\tilde{\alpha} s(t - \rho_0 \cos\varphi) e^{j2\pi t \rho_0 \sin\varphi}\}, \quad (13)$$

where we used the notation $\tilde{\alpha} = e^{-j2\pi(\rho_0^2/2)\cos\varphi\sin\varphi}$, as for the FrFT of $s(t)$ (and of $m(t)$) it can be substituted into the constant term of the received signal $\alpha_0$ with no loss of generality. Given the property (13) of FrFT and comparing it to (4), the relation of the FrFT parameters to the waveform and radar parameters can be found by:

$$\begin{cases} \rho_0 \cos\varphi = \dfrac{\tau_0}{T\gamma_{\mathrm{r}}}; \\ \rho_0 \sin\varphi = \dfrac{\beta\tau_0}{f_s}, \end{cases} \quad (14)$$

where $\gamma_{\mathrm{r}}$ is the oversampling factor for range processing. It should also be noted that depending on the sign of the analytical signal in (1) and also on the choice of up/down chirp, the beat frequency can have a negative sign. That should be taken in the account at the output of IQ demodulation. Furthermore, the angle of FrFT is fully determined by the parameters of the radar according to the ratio of scales in relative frequency shift ($\beta\tau_0/f_s$) to relative time delay of the signal ($\tau_0/T$) and thus:

$$\varphi = \arctan\left(\frac{B\gamma_{\mathrm{r}}}{f_s}\right). \quad (15)$$

The target range depends linearly on the parameter $\rho_0$:

$$\rho_0 = \frac{\tau_0}{T\gamma_{\mathrm{r}}\cos(\arctan\varphi)} = \frac{\sqrt{\varphi^2+1}}{T\gamma_{\mathrm{r}}}\tau_0, \quad (16)$$

and can be directly scaled to the range axis.

The structure of the FrFT receiver is presented in Fig. 2. The key component of the receiver is the fractional correlation block, which is reflected in (11).

It is assumed that fractional correlation block operates with the sampled signals. The discrete version of FrFT (12) can be derived from the discrete Fourier transform by eigenvalue decomposition of the transformation matrix [17], [28] and maintain most of the properties of continuous FrFT. It approximates well the continuous fractional Fourier transform for a large number of samples. Ozaktas *et al.* [19] proposed a faster way to compute an approximation of the continuous fractional Fourier. It exploits the fact that FrFT can be rewritten via a convolution in between two chirp multiplications, which need to be sampled at twice the original sampling rate. The computational complexity of such implementation is $\mathcal{O}(N\log_2 N)$, being determined by the realization of the convolution via FFT [19], [28]. The low computational load and high accuracy made this algorithm a common tool in digital signal processing [17].

It should be noted that the digital calculation of FrFT assumed that the signal is approximately confined to the interval $[-T/2, T/2]$ in time and to the interval $[-f_{\mathrm{s}}/2, f_{\mathrm{s}}/2]$ in frequency. Although the former is easy to satisfy by shifting the time axes of the Rx signal $s(t)$ and the replica $m(t)$ by $-T/2$, breaking the latter assumption results in folding the signal in FrFT domain for $f_{\mathrm{b}} > f_{\mathrm{s}}/2$. To avoid frequency folding, we propose to transmit the modulated signal $m(t)$ with a frequency offset $\Delta_{\mathrm{f}} = -f_{\mathrm{s}}/2 + B_{\mathrm{m}}/2$, where $B_{\mathrm{m}}$ is the bandwidth of modulation sequence, which insures that the sampled received signal is a time-frequency shifted version of the reference one for ranges:

$$r \in \left[0, \frac{(f_{\mathrm{s}} - B_{\mathrm{m}})T}{\Delta_{\mathrm{r}}}\right], \quad (17)$$

where $\Delta_{\mathrm{r}} = c/(2B)$. This criteria for the maximum range is defined assuming that for proper correlation the spectrum of the modulation signal defined by $B_m$ should fall below the cut-off frequency of the low-pass filter before ADC. Targets at longer ranges can still be observed, but they will have a larger SNR loss and significant distortion of the range profile. Modulation of FMCW therefore leads to the degradation of the maximum detectable range by the factor $(f_{\mathrm{s}} - B_{\mathrm{m}})/f_{\mathrm{s}}$. Note that the discussion above assumes the IQ receiver structure; if sampling only the I channel, both signals should belong to the interval $[0, f_{\mathrm{s}}/2]$ and thus the frequency offset should be set to $\Delta_{\mathrm{f}} = B_{\mathrm{m}}/2$.

## IV. Simulations

Consider the waveform with chirp bandwidth $B = 200$ MHz, chirp duration $T = 12.8$ $\mu$s operating at carrier $f_{\mathrm{c}} = 77$ GHz and the sampling frequency of the beat signal is $f_{\mathrm{s}} = 20$ MHz. With this setup, the maximum range of FMCW is $R_{\max} = 192$ m. The signal $m(t)$ is the Gaussian minimum shift keying (GMSK) modulated waveform with the time-bandwidth product of GMSK equal to 0.3 [29] and $N = 64$ chips, which corresponds to the modulation signal bandwidth of $B_{\mathrm{m}} = f_{\mathrm{s}}/4 = 5$ MHz. For range processing, we consider range oversampling $\gamma_{\mathrm{r}} = 2$, which according to (15) gives $\varphi = \arctan(20) \approx 1.52$. To demonstrate the principle of the FrFT receiver, we assume a noise-free scenario with a single stationary point-like target at the range $r_0 = 60$ m from the radar.

### A. Principles of FRFT receiver

The signal representations at all the stages of the fractional correlation (11) are plotted in Fig. 3. Here, we did not apply the frequency shift of the modulation signal, described at the end of the previous section, for better visibility (there is no difference in applying this shift or not for a target at $r_0 \leq R_{\max}/2$). It can be seen that despite the time and frequency

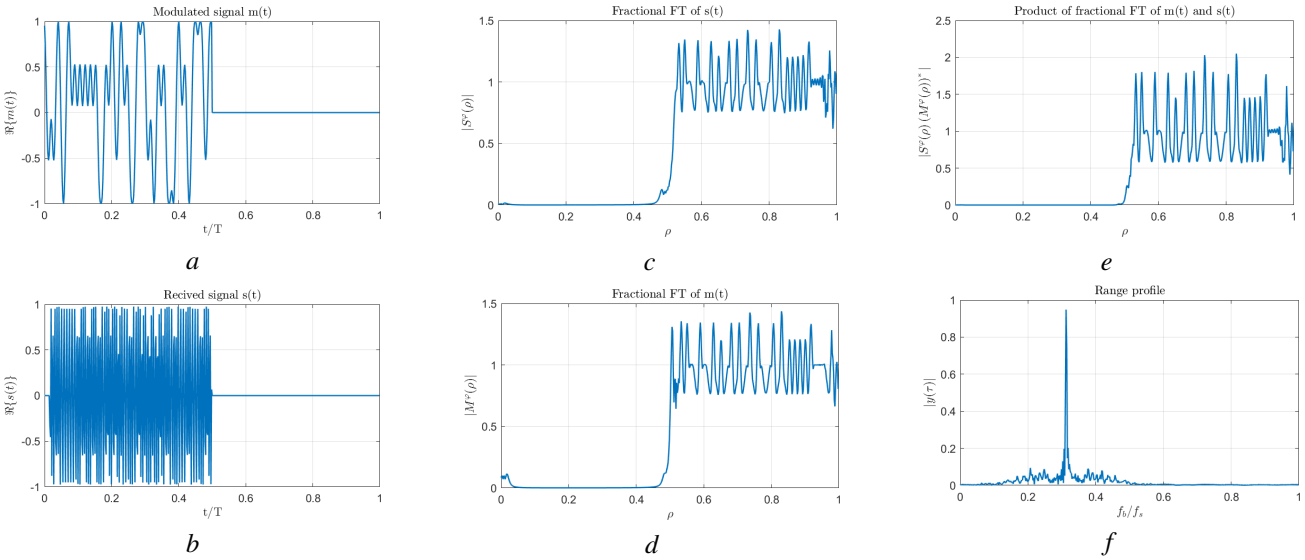


Fig. 3. (*a*) GMSK modulation signal (real part) $\Re\{m(t)\}$ ; (*b*) Received signal (real part) $\Re\{s(t)\}$; (*c*) FrFT of the modulation signal $M^{\frac{\pi}{2}+\phi}(\rho)$; (*d*) FrFT of the received signal $S^{\frac{\pi}{2}+\phi}(\rho)$; (*e*) Product of FrFTs $S^{\frac{\pi}{2}+\varphi}(\rho)\left(M^{\frac{\pi}{2}+\varphi}(\rho)\right)^*$; (*f*) Range profile as the result of fractional correlation (11).

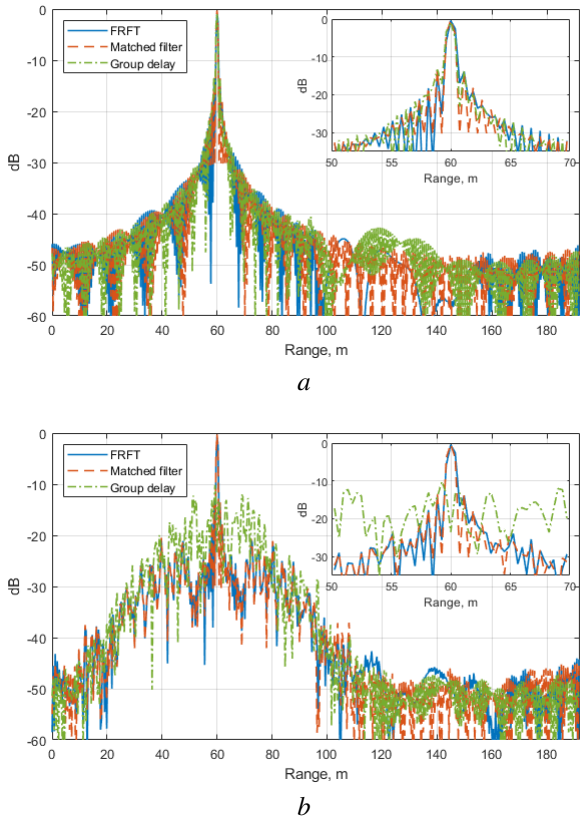


Fig. 4. Estimated range profile of a point-like target with three receiver structures considered: (*a*) narrow-band modulation, $B_\mathrm{m}/f_\mathrm{s} = 1/64$; (*b*) wide-band modulation, $B_\mathrm{m}/f_\mathrm{s} = 1/4$.

shift between the received $s(t)$ and the reference $m(t)$ signals (Fig. 3, *a, b*), it vanishes in their FrFT representations (Fig. 3, *c, d*). As a result, their product has a wide and uniform spectrum (Fig. 3, *e*), which leads to to narrow peak in the reconstructed range profile (Fig. 3, *f*).

We further compare the performance of the FrFT receiver to that of the filter bank approach, described in Section II-B (or compensated stretch processing [5], [6]) and to that of the group delay receiver [7], [9] (Fig. 4). Simulation results demonstrate that all three receivers have comparable range response for small bandwidth of modulation signal $B_\mathrm{m}/f_\mathrm{s} = 1/64$ (Fig. 4, *a*), but for larger bandwidth of $m(t)$ the performance of group delay receiver degrades significantly compared to that of filter bank and FrFT approaches (Fig. 4, *b* shows the result for $B_\mathrm{m}/f_\mathrm{s} = 1/4$). The performance of FrFT receiver is similar to that of the filter bank, being different only in the implementation and related to it computational complexity, as we mentioned above.

### *B. Processing loss*

To better demonstrate the limit of applicability of the group delay receiver, we compare in Fig. 5 the processing loss as the function of the code bandwidth $B_\mathrm{m}/f_\mathrm{s}$ normalized by $f_\mathrm{s}$. Similarly to the above, we considered a noise-free scenario with a single target present in the scene in the range $r_0 = 60 + w_\mathrm{r}$ m, where $w_\mathrm{r} \in [-2.5\Delta_\mathrm{r}, 2.5\Delta_\mathrm{r}]$, models an offset from the defined range grid with a step $0.125\Delta_\mathrm{r}$. The plots in Fig. 5 show the average (solid line), the best-case and the worst-case (dashed lines) processing loss for three considered receivers. It comprises the attenuation of the signal by the low-pass filter (LPF) prior to ADC and straddle loss: the mean value indicates the loss due to filtering of the received signal band by LPF prior to ADC sampling in the stretch processing architecture. The gap between lower and upper limits shows the bounds of the straddle loss, that can occur due to off-grid sampling. It can be seen that all three receivers

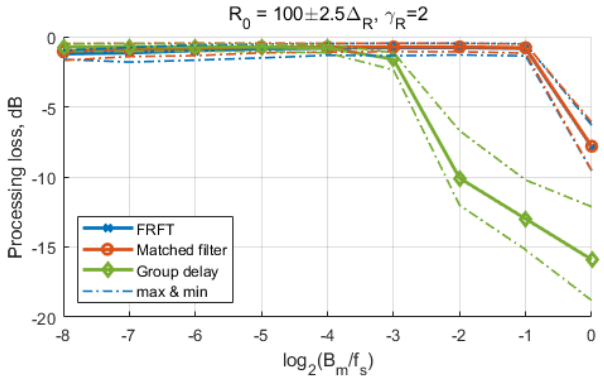


Fig. 5. Processing loss vs the normalized bandwidth of the modulation signal $m(t)$

behave similarly for a small code bandwidth: the straddle loss is about 1 dB [30]. For large code bandwidth $B_{\rm m}/f_{\rm s} \geq 1/8$, the degradation of the matched filter and the FrFT receiver is dominated by the straddle loss, while the group delay filter leads to a significant (over 10 dB) processing loss, which is also seen via defocusing of the main lobe of the range response in Fig. 4, *b*. This performance degradation of the group delay receiver for large bandwidth of the modulation signal $m(t)$, previously mentioned in [9], imposes an additional constraint on the choice of the modulation sequence $m(t)$. Finally, it should be noticed that for $B_{\rm m}/f_{\rm s} = 1$ all the receivers have degraded performance for observing the target at $r_0 \approx 60$, because a part of the modulated signal spectrum is being rejected by the low-pass filter of the receiver.

The bandwidth of the modulation signal has an impact on the maximum detectable target range. We investigate this behavior via simulations in Fig. 6 for three values of the normalized bandwidth of the modulation signal: $B_{\rm m}/f_{\rm s} = 1/16$ (Fig. 6, *a*), $B_{\rm m}/f_{\rm s} = 1/4$ (Fig. 6, *b*) and $B_{\rm m}/f_{\rm s} = 1/2$ (Fig. 6, *c*). The range axes in Fig. 6 are similar to that in Fig. 4, up to the normalization by a scalar $R_{\max}$. It can be seen, that a small bandwidth of the modulation $B_{\rm m}$ (Fig. 6, *a*) has almost no impact on the maximum detectable range of the target, while in the case of a significant modulation bandwidth $B_{\rm m}$, processing loss rapidly increases for $r \geq 0.8R_{\max}$ when $B_{\rm m}/f_{\rm s} = 1/4$ and for $r \geq 0.6R_{\max}$ when $B_{\rm m}/f_{\rm s} = 1/2$. These values slightly exceed the criteria defined in (17), while the latter still gives a reasonable estimation of the maximum range for applying dechirping receiver with a modulated LFM waveform.

### C. Range-Doppler processing

We further demonstrate the performance of the proposed receiver by comparing range-Doppler images of three receiver structures, presented above. For this simulation, we assume the radar transmits $M = 128$ chirps with the parameters, mentioned above and pulse repetition interval (PRI) $T_r = T$. Each chirp is modulated with a different random GMSK modulation with $B_m = f_s/4 = 5$ MHz. Two targets resulting in equal Rx power are present in the scene: $r_0 = 60$ m and Doppler frequency $f_{\rm D,0} = 5$ KHz; $r_1 = 75$ m $f_{\rm D,1} = -20$

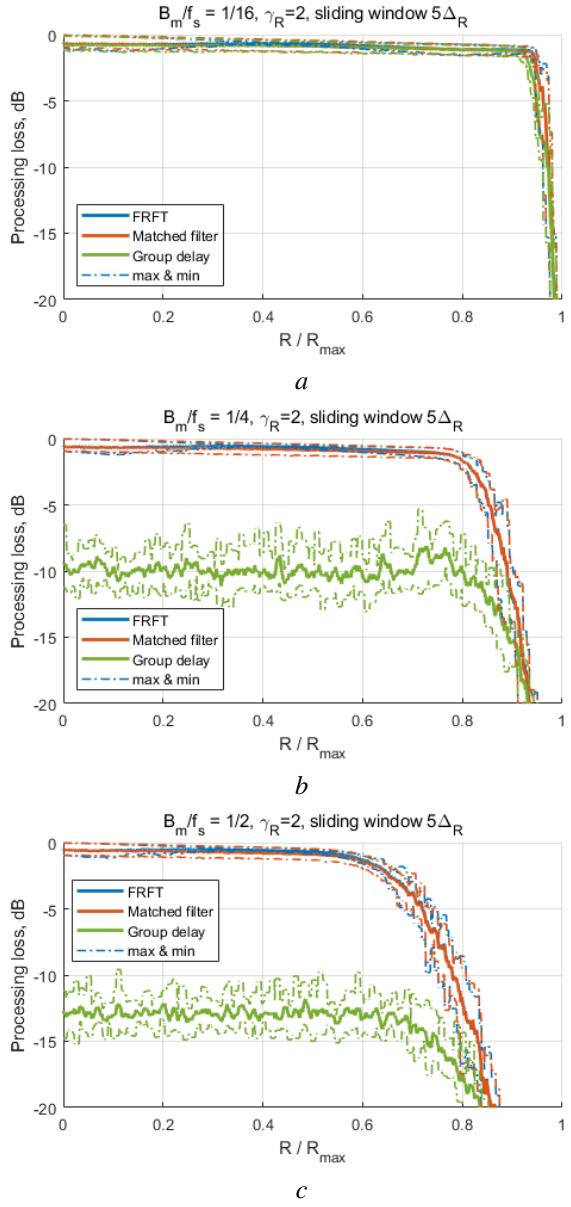


Fig. 6. Processing loss as a function of the target range: (*a*) narrow-band modulation, $B_{\rm m}/f_{\rm s} = 1/16$; (*b*) wide-band modulation, $B_{\rm m}/f_{\rm s} = 1/4$, (*c*) $B_{\rm m}/f_{\rm s} = 1/2$.

KHz. The proposed processing is applied per chirp, followed by a Doppler FFT with Hamming window to reduce Doppler sidelobes. Range-Doppler maps of the FRFT receiver, the matched filter bank and the group delay receiver are demonstrated in Fig. 7, *a, b, c*, respectively. The FRFT receiver and the matched filter bank indicate the responses of both targets at their correct positions and provide about 50 dB dynamic range (21 dB slow-time gain and about 30 dB per chirp, see 4, *b*), which significantly outperforms the group delay receiver.

### D. Computational complexity

Further, we compared the average over 100 trials execution time of each of the three receivers (for a single chirp) as the function of fast-time samples per chirp (Fig. 8). In this simulation, we used two different implementations of FrFT:

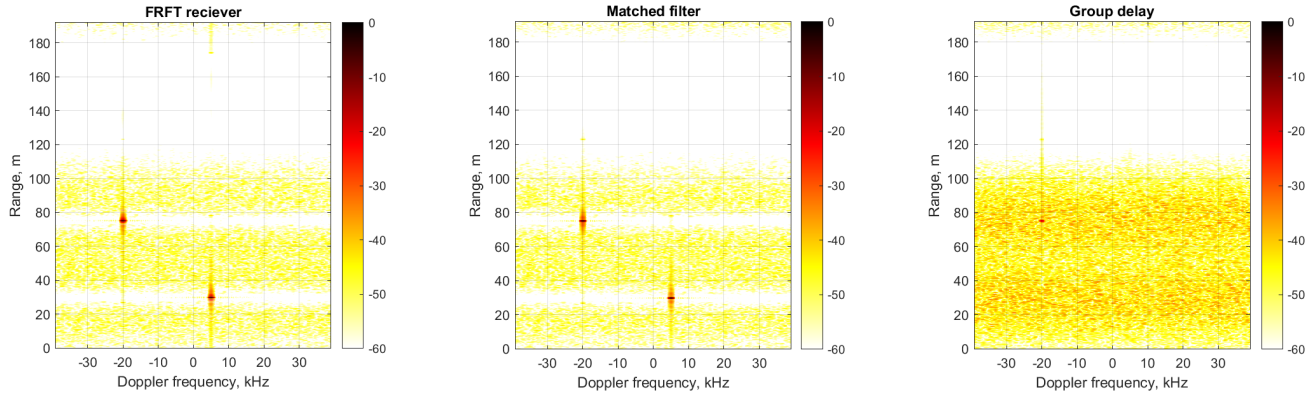


Fig. 7. Range-Doppler processing: (*a*) FRFT receiver; (*b*) Matched filter bank; (*c*) Group delay receiver.

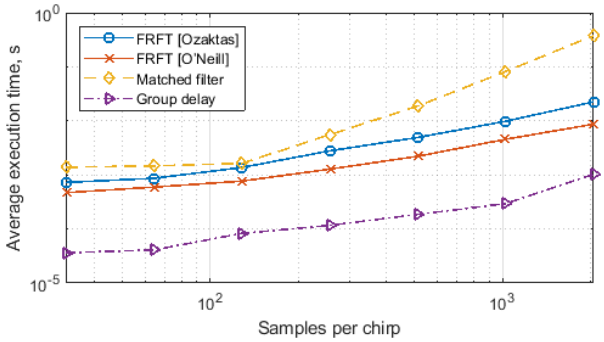


Fig. 8. Computational complexity of three considered receiver structures

`fracF` – the direct implementation of algorithm [19] in MATLAB by Ozaktas *et al.* and `fracFT` – the implementation of FrFT [19] by J. O'Neill [31]. The difference between these implementations is discussed in detail in [28].

The results in Fig. 8 show that the slope of the FrFT and group delay receivers follows the trend $\mathcal{O}(N\log_2(N))$ and the complexity of the matched filter increases according to $\mathcal{O}(N^2)$. Two implementations of FrFT have slightly different execution time: the one by J. O'Neill [31] being more efficient. For a moderate to large number of samples per chirp, the FrFR receiver has a gain of more than one order of magnitude in computational time. The group delay receiver reduces the execution time even more, but its performance for long code sequences is unsatisfactory, as explained above.

## V. Experimental validation

The experimental validation of the proposed processing technique was performed with PARSAX radar [32], installed on the rooftop of 100 m high EEMCS (Electrical Engineering, Mathematics and Computer Science) building of the Delft University of Technology. The radar was pointing to the top of an industrial chimney, located about 1185 m away from the radar. A single (HH) polarimetric channel was used for the measurements. The waveforms settings are: $f_\mathrm{c} = 3.315$ GHz, $B = 40$ MHz, $T_\mathrm{r} \approx 1$ ms; $m(t)$ is a binary phase-shift keying (BPSK) sequence with $B_\mathrm{m} \approx 1$ MHz. The raw data was collected at the intermediate frequency $f_\mathrm{IF} = 125$ MHz, followed by the downconversion to the baseband, deramping (this and the following steps are not applied for the full band matched filter processing, considered below), downsampling to $f_\mathrm{s} \approx 4.2$ Mhz (corresponding to 4096 range cells), and applying one of the considered range processing techniques. Chebyshev windowing with 80 dB sidelobe level and range oversampling with $\gamma_\mathrm{r} = 4$ are applied for all the techniques (for the IFFT in (11)). The results demonstrated in Fig. 9 compare the performance of the fractional correlator (11), matched filter bank after deramping (8), group delay receiver [9] and the matched filtering in the full band. The results demonstrate that the group delay filter performs poorly with the selected bandwidth of the code, while the other techniques demonstrate similar performance. This comes with the high sampling rate requirements of the full-band matched filtering and low computational efficiency of the matched filter bank after deramping (8). The proposed fractional correlator obtains the same result with low ADC sampling and computational complexity requirements.

## VI. Conclusion

In this paper, we proposed the new receiver structure for the modulated LFM waveform, which can be realized in simple hardware and requires computational resources similar to FFT. We demonstrated that matched filter processing of this waveform corresponds to calculating the cross-correlation along a diagonal line in the delay-Doppler plane - called Fractional correlation, which can be efficiently implemented via the Fractional Fourier Transform (FrFT). The receiver, based on the proposed principle, offers a significant improvement over the state-of-the-art techniques for moderate-to-large bandwidths of modulation signals, as demonstrated via numerical simulations and experimental processing from waveform-agile radar PARSAX.

## Acknowledgment

The authors would like to thank Utku Kumbul and Fred van der Zwan for conducting the measurements and sharing the experimental data.

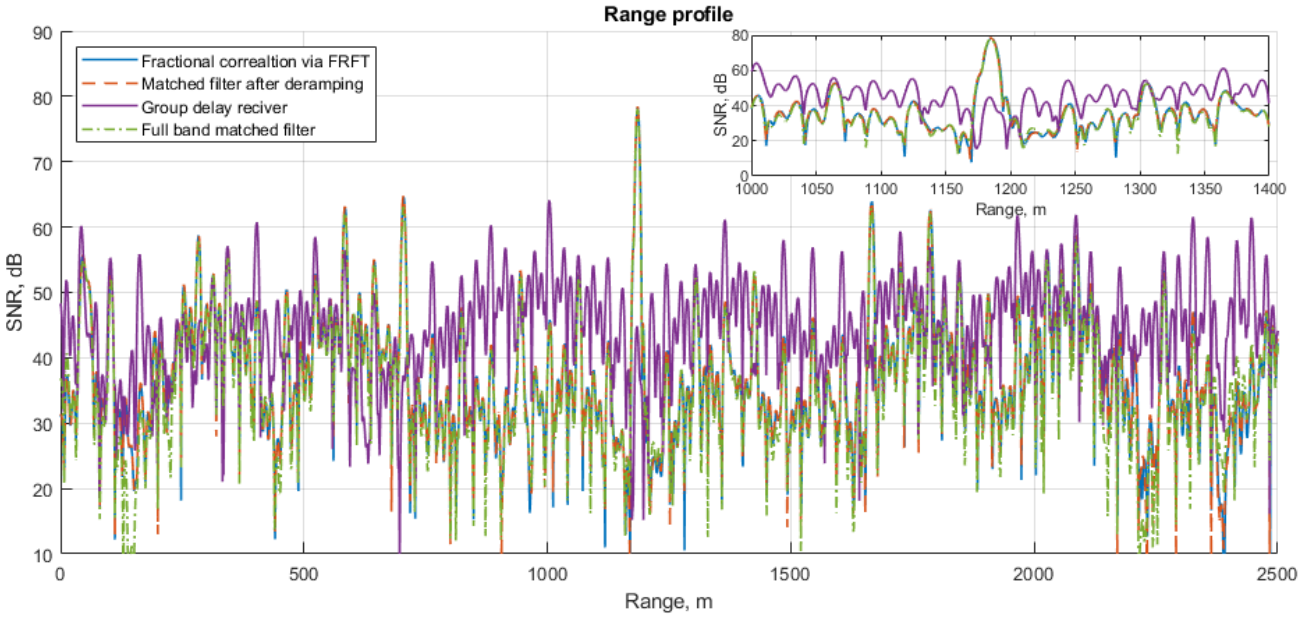


Fig. 9. Measured range profile of a chimney at $r \approx 1185$ m, illuminated by a BPSK modulated chirp

## REFERENCES


[1] H. Sun, F. Brigui, and M. Lesturgie, "Analysis and comparison of MIMO radar waveforms," in *2014 International Radar Conference*. IEEE, 2014, pp. 1–6.

[2] J. de Wit, W. van Rossum, and A. de Jong, "Orthogonal waveforms for FMCW MIMO radar," in *IEEE 2011 Radar Conference (RADAR), 23-27 May 2011, Kansas City, MO, USA*, 2011, p. 686.

[3] J. Reneau and R. R. Adhami, "Phase-coded LFMCW waveform analysis for short range measurement applications," in *2014 IEEE Aerospace Conference*. IEEE, 2014, pp. 1–6.

[4] M. Nowak, M. Wicks, Z. Zhang, and Z. Wu, "Co-designed radar-communication using linear frequency modulation waveform," *IEEE Aerospace and Electronic Systems Magazine*, vol. 31, no. 10, pp. 28–35, 2016.

[5] P. M. McCormick, C. Sahin, S. D. Blunt, and J. G. Metcalf, "FMCW implementation of phase-attached radar-communications (PARC)," in *2019 IEEE Radar Conference (RadarConf)*. IEEE, 2019, pp. 1–6.

[6] D. M. Hemmingsen, P. M. McCormick, S. D. Blunt, C. Allen, A. Martone, K. Sherbondy, and D. Wikner, "Waveform-diverse stretch processing," in *2018 IEEE Radar Conference (RadarConf18)*. IEEE, 2018, pp. 0963–0968.

[7] F. Uysal, "Phase-coded FMCW automotive radar: System design and interference mitigation," *IEEE Transactions on Vehicular Technology*, vol. 69, no. 1, pp. 270–281, 2019.

[8] ——, "Phase coded frequency modulated continuous wave (FMCW) radar system," February 2019, patent Number NL2020050066W, and WO2020162751A1.

[9] F. Lampel, R. F. Tigrek, A. Alvarado, and F. M. Willems, "A performance enhancement technique for a joint FMCW radcom system," in *2019 16th European Radar Conference (EuRAD)*. IEEE, 2019, pp. 169–172.

[10] F. G. Jansen, F. Laghezza, and F. Lampel, "Radar-based communication," August 2020, united States Patent Application Number US2020256948A1.

[11] A. Meta, P. Hoogeboom, and L. P. Ligthart, "Signal processing for FMCW SAR," *IEEE Transactions on Geoscience and Remote Sensing*, vol. 45, no. 11, pp. 3519–3532, 2007.

[12] H. Krichene, E. Brawley, K. Lauritzen, A. Wu, and S. Talisa, "Time sidelobe correction of hardware errors in stretch processing," *IEEE Transactions on Aerospace and Electronic Systems*, vol. 48, no. 1, pp. 637–647, 2012.

[13] Y.-X. Zhang, R.-J. Hong, P.-P. Pan, Z.-M. Deng, and Q.-F. Liu, "Frequency-domain range sidelobe correction in stretch processing for wideband LFM radars," *IEEE Transactions on Aerospace and Electronic Systems*, vol. 53, no. 1, pp. 111–121, 2017.

[14] F. Laghezza and F. Lampel, "Predistortion technique for joint radar/communication systems," November 2021, european Patent Number EP3907520A1.

[15] U. Kumbul, N. Petrov, C. S. Vaucher, and A. Yarovoy, "Smoothed phase-coded fmcw: Waveform properties and transceiver architecture," *IEEE Transactions on Aerospace and Electronic Systems*, pp. 1–18, 2022.

[16] D. Schindler, B. Schweizer, C. Knill, J. Hasch, and C. Waldschmidt, "MIMO-OFDM radar using a linear frequency modulated carrier to reduce sampling requirements," *IEEE Transactions on Microwave Theory and Techniques*, vol. 66, no. 7, pp. 3511–3520, 2018.

[17] R. Tao, B. Deng, and Y. Wang, "Research progress of the fractional Fourier transform in signal processing," *Science in China Series F*, vol. 49, no. 1, pp. 1–25, 2006.

[18] Z. Xinghao and T. Ran, "The new algorithm for passive radar MTD based on the fractional correlation," in *Proceedings 7th International Conference on Signal Processing, 2004. Proceedings. ICSP'04. 2004.*, vol. 3. IEEE, 2004, pp. 2061–2065.

[19] H. M. Ozaktas, O. Arikan, M. A. Kutay, and G. Bozdagt, "Digital computation of the fractional Fourier transform," *IEEE Transactions on signal processing*, vol. 44, no. 9, pp. 2141–2150, 1996.

[20] M. I. Skolnik, *Radar handbook*. McGraw-Hill Education, 2008.

[21] N. Levanon and E. Mozeson, *Radar signals*. John Wiley & Sons, 2004.

[22] S. W. Smith *et al.*, *The scientist and engineer's guide to digital signal processing*. California Technical Pub. San Diego, 1997.

[23] L. B. Almeida, "The fractional Fourier transform and time-frequency representations," *IEEE Transactions on signal processing*, vol. 42, no. 11, pp. 3084–3091, 1994.

[24] O. Akay and G. F. Boudreaux-Bartels, "Fractional convolution and correlation via operator methods and an application to detection of linear FM signals," *IEEE Transactions on signal processing*, vol. 49, no. 5, pp. 979–993, 2001.

[25] E. Sejdić, I. Djurović, and L. Stanković, "Fractional Fourier transform as a signal processing tool: An overview of recent developments," *Signal Processing*, vol. 91, no. 6, pp. 1351–1369, 2011.

[26] X. Chen, J. Guan, N. Liu, and Y. He, "Maneuvering target detection via Radon-fractional Fourier transform-based long-time coherent integration," *IEEE Transactions on Signal Processing*, vol. 62, no. 4, pp. 939–953, 2014.

[27] D. Gaglione, C. Clemente, C. V. Ilioudis, A. R. Persico, I. K. Proudler, J. J. Soraghan, and A. Farina, "Waveform design for communicating radar systems using fractional Fourier transform," *Digital Signal Processing*, vol. 80, pp. 57–69, 2018.

[28] A. Bultheel and H. E. M. Sulbaran, "Computation of the fractional Fourier transform," *Applied and Computational Harmonic Analysis*, vol. 16, no. 3, pp. 182–202, 2004.

[29] J. B. Anderson, T. Aulin, and C.-E. Sundberg, *Digital phase modulation*. Springer Science & Business Media, 2013.
[30] M. A. Richards, J. Scheer, W. A. Holm, and W. L. Melvin, *Principles of modern radar*. Citeseer, 2010.
[31] J. C. O'Neill, "Discrete TFDs: Time-frequency analysis software," http://tfd.sourceforge.net/.
[32] O. A. Krasnov, L. P. Ligthart, Z. Li, G. Babur, Z. Wang, and F. van der Zwan, "PARSAX: High-resolution Doppler-polarimetric FMCW radar with dual-orthogonal signals," in *18-th International Conference on Microwaves, Radar and Wireless Communications*. IEEE, 2010, pp. 1–5.

**Nikita Petrov** received his engineering degree in radio-electronic control systems from Baltic State Technical University "VOENMEH", Saint-Petersburg, Russia in 2012, and his PhD degree in radar signal processing from Delft University of Technology, the Netherlands, in 2019. Since then he stays as a postdoctoral researcher with the Microwave Sensing, Signals and Systems (MS3) Section, Faculty of Electrical Engineering, Mathematics, and Computer Science (EEMCS), Delft University of Technology. His research interests include modern radar technologies, radar signal processing, multi-channel and multi-band signals and systems, high resolution and automotive radars. Since 2022 he is with NXP Semiconductors, Eindhoven, The Netherlands. Dr. Petrov currently serves as a reviewer for IEEE Transactions on Aerospace and Electronic Systems and IEEE Transactions on Geoscience and Remote Sensing.

**Alexander G. Yarovoy** (FIEEE' 2015)graduated from the Kharkov State University, Ukraine, in 1984 with the Diploma with honor in radiophysics and electronics. He received the Candidate Phys. Math. Sci. and Doctor Phys. Math. Sci. degrees in radiophysics in 1987 and 1994, respectively. In 1987 he joined the Department of Radiophysics at the Kharkov State University as a Researcher and became a Full Professor there in 1997. From September 1994 through 1996 he was with Technical University of Ilmenau, Germany as a Visiting Researcher. Since 1999 he is with the Delft University of Technology, the Netherlands. Since 2009 he leads there a chair of Microwave Sensing, Systems and Signals. His main research interests are in high-resolution radar, microwave imaging and applied electromagnetics (in particular, UWB antennas). He has authored and co-authored more than 500 scientific or technical papers, seven patents and fourteen book chapters. He is the recipient of the European Microwave Week Radar Award for the paper that best advances the state-of-the-art in radar technology in 2001 (together with L.P. Ligthart and P. van Genderen) and in 2012 (together with T. Savelyev). In 2010 together with D. Caratelli Prof. Yarovoy got the best paper award of the Applied Computational Electromagnetic Society (ACES). Prof. Yarovoy served as the General TPC chair of the 2020 European Microwave Week (EuMW'20), as the Chair and TPC chair of the 5th European Radar Conference (EuRAD'08), as well as the Secretary of the 1st European Radar Conference (EuRAD'04). He served also as the co-chair and TPC chair of the Xth International Conference on GPR (GPR2004). He served as an Associated Editor of the International Journal of Microwave and Wireless Technologies from 2011 till 2018 and as a Guest Editor of five special issues of the IEEE Transactions and other journals. In the period 2008-2017 Prof. Yarovoy served as Director of the European Microwave Association (EuMA).